Check for updates

ADVANCED HEALTHCARE MATERIALS
www.advhealthmat.de

Tabletized Supramolecular Assemblies for Sublingual Peptide Immunization

*Sean H. Kelly, Emmanuel E. Opolot, Yaoying Wu, Benjamin Cossette, Ajay K. Varadhan, and Joel H. Collier**

Widespread vaccination is essential to global health. Significant barriers exist to improving vaccine coverage in lower- and middle-income countries, including the costly requirements for cold-chain distribution and trained medical personnel to administer the vaccines. A heat-stable and highly porous tablet vaccine that can be administered sublingually via simple dissolution under the tongue is described. SIMPL tablet vaccines (Supramolecular IMmunization with Peptides subLingually) are produced by freeze-drying a mixture of self-assembling peptide-polymer nanofibers, sugars, and adjuvant. Sublingual immunization with SIMPL tablets raises antibody responses against both a model epitope from ovalbumin and a clinically relevant epitope from *Mycobacterium tuberculosis*. Further, sublingual antibody responses are not diminished after heating the tablets for 1 week at 45 °C, in contrast to a more conventional carrier vaccine (KLH). This approach directly addresses the need for a heat-stable and easily deliverable vaccine to improve equity in global vaccine coverage.

Global vaccination coverage against infectious diseases in lower- and middle-income countries still lags behind higher-income countries, resulting in preventable deaths.[1] Improving global vaccine coverage is a complex and multifaceted challenge, a major component of which is the chain of distribution.[2] Vaccines must be transported and stored within a continuous cold-chain near 4 °C to prevent loss of potency,[3] but poorly maintained equipment and unreliable electricity grids in lower- and middle-income countries make such transport difficult.[2] Inequities of distribution occur even within countries due to transportation costs and proximity to health care facilities where trained personnel can safely administer the vaccines.[4] A heat-stable and self-deliverable vaccine would directly address these challenges.

Sublingual vaccine delivery (under the tongue) is needle-free and has the potential for self-administration,[5–6] making it an ideal route for global vaccine distribution. Vaccines based on chemically defined biomaterials are increasingly being considered for infectious diseases[7–9] and have the potential for greater thermal stability than traditional vaccines based on attenuated pathogens. Despite this, sublingual biomaterial vaccines remain relatively unexplored due in part to challenges of delivery through the salivary mucus layer. Sublingual vaccine materials are taken up by dendritic cells in the mucosal tissue below the epithelium, which transport them to the cervical lymph nodes to prime immune responses.[10] The mucus layer above the epithelium is a significant barrier, as it can ensnare vaccine materials through polyvalent, low-affinity adhesive interactions.[11] We recently reported the design of a sublingual nanofiber vaccine based on self-assembling Q11 peptides conjugated to mucus-inert materials such as polyethylene glycol (PEG) or random sequences of proline, alanine, and serine (PAS).[12] Here, we designed a process to tabletize these nanofibers, producing a first-of-its-kind, heat-stable, and easily-administrable SIMPL (Supramolecular IMmunization with Peptides sublingually) tablet vaccine that dissolves under the tongue.

In designing this tablet vaccine, we sought to meet the key design criteria of structural integrity for handleability, microscale porosity for promoting dissolution, and preservation of nanofiber structure for immunogenicity. We focused on a freeze-dried tabletization process, adopting the use of sugar excipients from pharmaceutical tablet production.[13] We selected mannitol and dextran to promote tablet strength and porosity[14–15] and trehalose as a cryoprotectant to aid in retaining nanofiber morphology.[16] We also included an adjuvant in the formulation due to our previous finding that this was needed for high-titer sublingual antibody responses with peptide nanofibers.[12] To control tablet size and shape, we 3D-printed a custom negative tablet mold, then made the final mold of flexible polydimethylsiloxane (PDMS) (Figure S1, Supporting Information). Freeze-dried SIMPL tablets were formed by mixing the sugars and adjuvant with fibrillized peptide-polymers, transferring the solution to the PDMS mold, and lyophilizing (**Figure 1**A).

The SIMPL tabletization process yielded tablets that were strong enough to be handled without breaking, fulfilling the bulk handleability requirement (Figure 1B). An effective tablet should quickly dissolve in the volume-limited sublingual space. MicroCT analysis of the tablet's microstructure showed a high-degree of

Dr. S. H. Kelly, E. E. Opolot, Dr. Y. Wu, B. Cossette, A. K. Varadhan, Prof. J. H. Collier
Biomedical Engineering Department
Duke University
Durham, NC 27708, USA
E-mail: joel.collier@duke.edu

The ORCID identification number(s) for the author(s) of this article can be found under https://doi.org/10.1002/adhm.202001614

DOI: 10.1002/adhm.202001614

 © 2021 Wiley-VCH GmbH

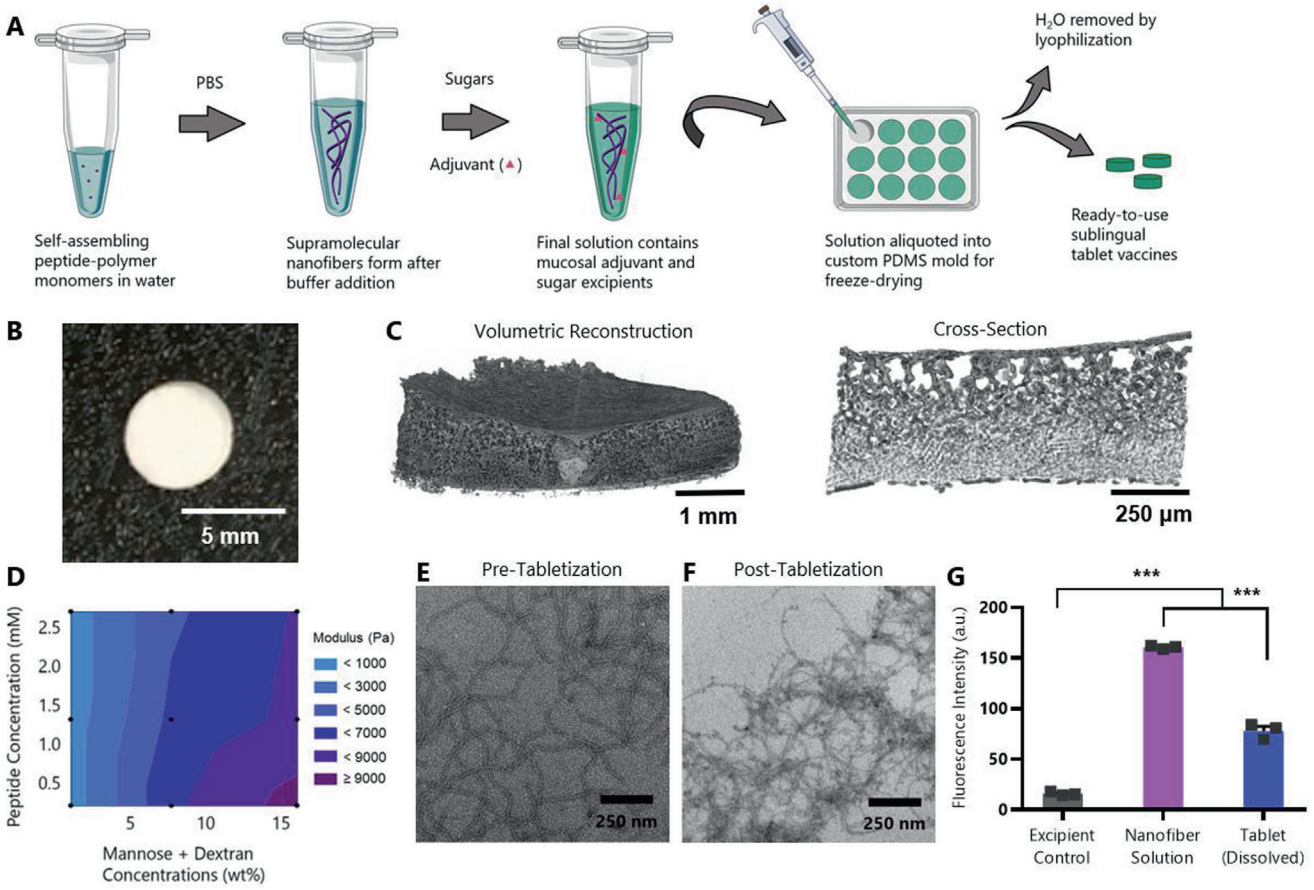

Figure 1. SIMPL tabletization process produces highly porous freeze-dried tablets that maintain nanofiber structure. A) Schematic illustrating production of SIMPL tablet vaccines. B) Camera image of tablet. C) Volumetric reconstruction and cross-section of tablet structure from microCT highlighting tablet porosity. D) Contour plot showing combined effects of peptide and sugar concentration in tablets on elastic modulus. Tablets were prepared at nine combinations of peptide (OVAQ11) and sugar (dextran and mannose) concentrations (black dots on plot) and subjected to compressive testing using a micro-strain analyzer. Trehalose concentration was held constant. $n = 3$ tablets/group, mean values shown. Individual graphs showing effects of sugar and peptide concentration individually are in Figure S2 (Supporting Information). E,F) TEM images of PEG-Q11OVA nanofibers prepared at 2×10^{-3} M (E) or a tablet dissolved at 2×10^{-3} M (F), each diluted to 0.2×10^{-3} M before imaging. G) β-sheet secondary structure was assessed by thioflavin T binding of a nanofiber solution before tabletization and of an equal concentration solution of a dissolved tablet. Excipient control contained no OVAQ11. *** $p < 0.001$ by 1-way ANOVA with Tukey's multiple comparisons test, n=3/group.

porosity qualitatively (Figure 1C). This large surface area allowed the tablets to dissolve rapidly in aqueous solvent (Movie S1, Supporting Information). Further, by modulating the concentrations of peptide and sugar within the tabletized solutions we could tune the elastic modulus of the resulting tablets (Figure 1D and Figure S2: Supporting Information). We do not expect the adjuvants utilized to affect moduli, owing to their comparably much lower concentrations. Previous work in our lab has shown that fibrillization is critical to the function of Q11-based vaccines.[17] We used electron microscopy to compare the structure of nanofibers before and after tabletization (Figure 1E,F). We immediately prepared TEM grids after dissolving tablets in PBS to prevent re-fibrillization over time from skewing the results. Nanofibers remained after tabletization, though they appeared slightly shorter by qualitative comparison. To corroborate this finding, we analyzed the extent of β-sheet secondary structure by Thioflavin T (ThT) binding (Figure 1G). ThT binding was reduced after tabletization, but remained significantly higher than vehicle controls. Taken together, these findings suggested that although the tabletization process diminished nanofiber structure to some extent, significant fibrillar morphology was retained within SIMPL tablets. We next sought to determine whether peptide nanofibers prepared in this way retained their immunogenicity.

An advantage of supramolecular vaccines is their ability to raise antibody responses against peptide epitopes, which are highly specific but poorly immunogenic.[18] We first tested the ability of tabletized supramolecular assemblies to raise responses against the model $OVA_{323\text{-}339}$ peptide (pOVA). Nanofibers assembled from OVA-Q11-PEG_{3000} (OVAQ11) were readily acquired when delivered to cultures of dendritic cells (**Figure 2**A). Unadjuvanted tabletized nanofibers also upregulated CD80, and to a lesser extent MHC-II, on dendritic cells in vitro, in contrast to non-tabletized nanofiber solutions (Figure S3, Supporting Information). For sublingual immunizations, we placed SIMPL tablets under the tongue of anesthetized C57BL/6 mice and allowed them to dissolve unaided (without the application of

© 2021 Wiley-VCH GmbH

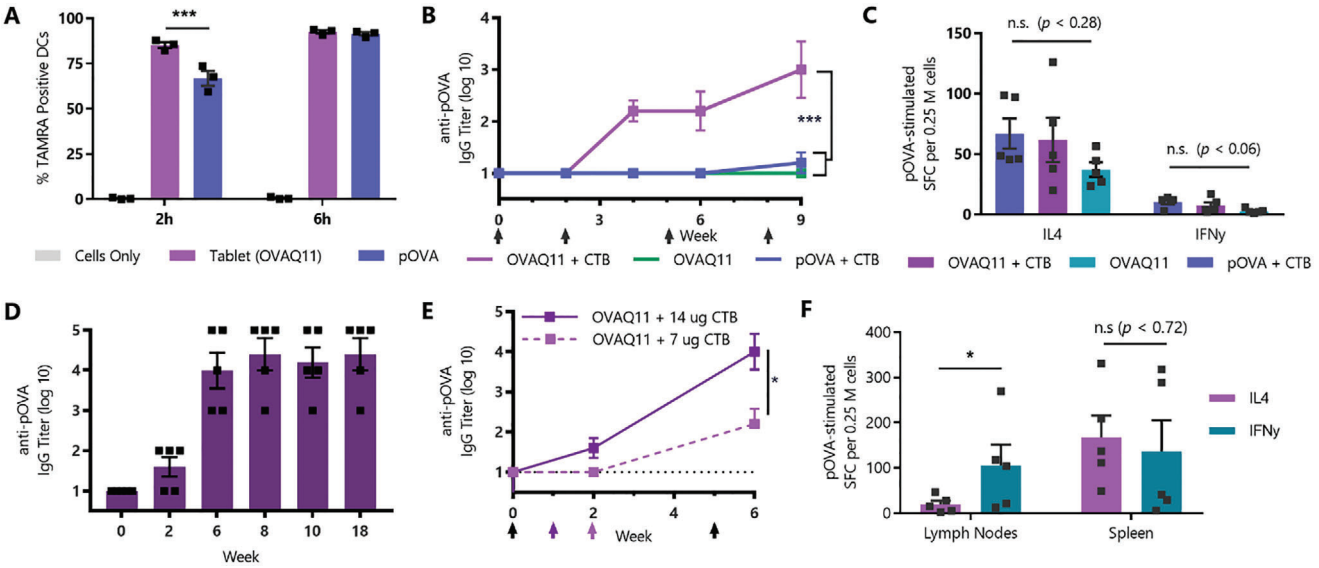

Figure 2. SIMPL tablets containing Q11-PEG assemblies raise antibody responses in an adjuvant dose-dependent manner. A) Fluorescently labelled TAMRA-pOVA peptide or SIMPL tablets prepared with TAMRA-OVAQ11 nanofibers were incubated with DC2.4 mouse dendritic cells, and uptake was measured by flow cytometry. ***$p < 0.001$ by 2-way ANOVA with Tukey's multiple comparisons test, $n = 3$/group. B) C57BL/6 mice were immunized sublingually with tablets containing 20 nmol of pOVA or OVAQ11 and 7 µg cholera toxin B adjuvant (CTB) and boosted at weeks 2, 5, and 8. *** $p < 0.001$ by 2-way ANOVA with Tukey's multiple comparisons test, $n = 5$/group. C) Mice from (B) were boosted at week 15 and sacrificed 7 days later. Spleens were harvested and T-cell responses were measured by ELISPOT. SFC: spot-forming cells. n.s. (not significant) by multiple 1-way ANOVAs, $n = 5$/group. Full ELISPOT results are in Figure S4 (Supporting Information). D) Mice were immunized sublingually with tablets containing 20 nmol OVAQ11-PEG and 14 µg CTB and boosted at weeks 1, 5, and 17. $n = 5$/group. E) Mice from OVAQ11 + CTB tablet groups in (B) and (D) were compared to show effect of adjuvant dose on titer. Color-coded arrows indicate boosting (black arrows indicate both groups were boosted). * $p < 0.05$ by 2-way ANOVA. F) Mice from (D) were sacrificed at week 18, spleens and draining lymph nodes (submandibular and cervical) were harvested, and T-cell responses were measured by ELISPOT. Full ELISPOT results are in Figure S5 (Supporting Information). * $p < 0.05$ by multiple *t*-tests with Holm-Šidák correction.

additional liquid). Mice immunized in this way with tablets containing nanofibers and the protein adjuvant cholera toxin B (CTB) raised epitope-specific IgG responses (Figure 2B). Notably, tablets that contained PEG-conjugated pOVA (non-assembling) rather than self-assembling OVAQ11 failed to raise responses, highlighting the importance of supramolecular assembly and suggesting the ability of the supramolecular tablet to preserve nanofiber structure. This is in line with previous work showing that assembly is essential for immunogenicity of subcutaneously delivered Q11 nanofibers[17] and sublingually delivered Q11-PEG solutions.[8] By contrast, T-cell responses were unaffected by the presence or absence of the Q11 assembly domain, with IL-4 dominant splenic responses observed for all groups (Figure 2C and Figure S4: Supporting Information).

To test the ability to modulate the antibody titer raised by the SIMPL sublingual tablet vaccine, we increased the CTB adjuvant dose from 7 µg per tablet to 14 µg per tablet (Figure 2D). Mice immunized with the higher adjuvant dose had significantly higher serum IgG titers after two boosts, with an increase in mean titer from 2.2 to 4 representing an over 60-fold change in antibody concentration (Figure 2E). The higher dose of CTB adjuvant also led to T-cell responses that were more balanced between IL-4 and IFNγ in the spleen (Figure 2F and Figure S5: Supporting Information), similar to previously published CTB-adjuvanted sublingual vaccines.[19] It is possible that at lower adjuvant doses, the Th2-bias of unadjuvanted Q11 vaccines[20] remains, but that at higher doses the effects of CTB are more pronounced. In contrast to the spleen, T-cell responses in the draining submandibular and cervical lymph nodes were more biased toward IFNγ (Figure 2F). This is perhaps due to CTB adjuvant draining to the lymph node, but future characterization of the T-cell response to SIMPL tablets is needed to address these questions.

Having established the immunogenicity of SIMPL tablets, we next investigated the important consideration of heat stability. Given the importance of thermal stability to equitable global vaccine distribution, we chose a peptide epitope from *Mycobacterium tuberculosis*. Tuberculosis is the leading cause of infectious death globally, with 97% of cases coming from low- and middle-income countries.[21] The selected peptide epitope from the 6 kDa early secretory antigenic target of *M. tuberculosis* (ESAT6) contains contiguous B- and T-cell epitopes and was a protective target in a preclinical model of tuberculosis infection.[22] In all experiments, heated groups were kept for one week at 45 °C, a temperature at which even relatively stable vaccines can lose potency.[23–24]

We compared the thermal stability of the tablet vaccine with a conventional peptide-carrier conjugate, keyhole limpet hemocyanin (KLH). Subcutaneous injection of CBA/J mice with KLH-ESAT6 and alum adjuvant led to strong antigen-specific antibody responses even after heating (**Figure 3**A). Strikingly, however, sublingually delivered KLH-ESAT6 with CTB adjuvant led to no detectable response after heating, highlighting the challenge of sublingual peptide immunization. By contrast, sublingual immunization with heated SIMPL tablets containing $mPEG_{2000}$-Q11ESAT6 nanofibers (Q11ESAT6) and CTB adjuvant raised IgG antibodies (Figure 3B). Most notably, there was no significant

 © 2021 Wiley-VCH GmbH

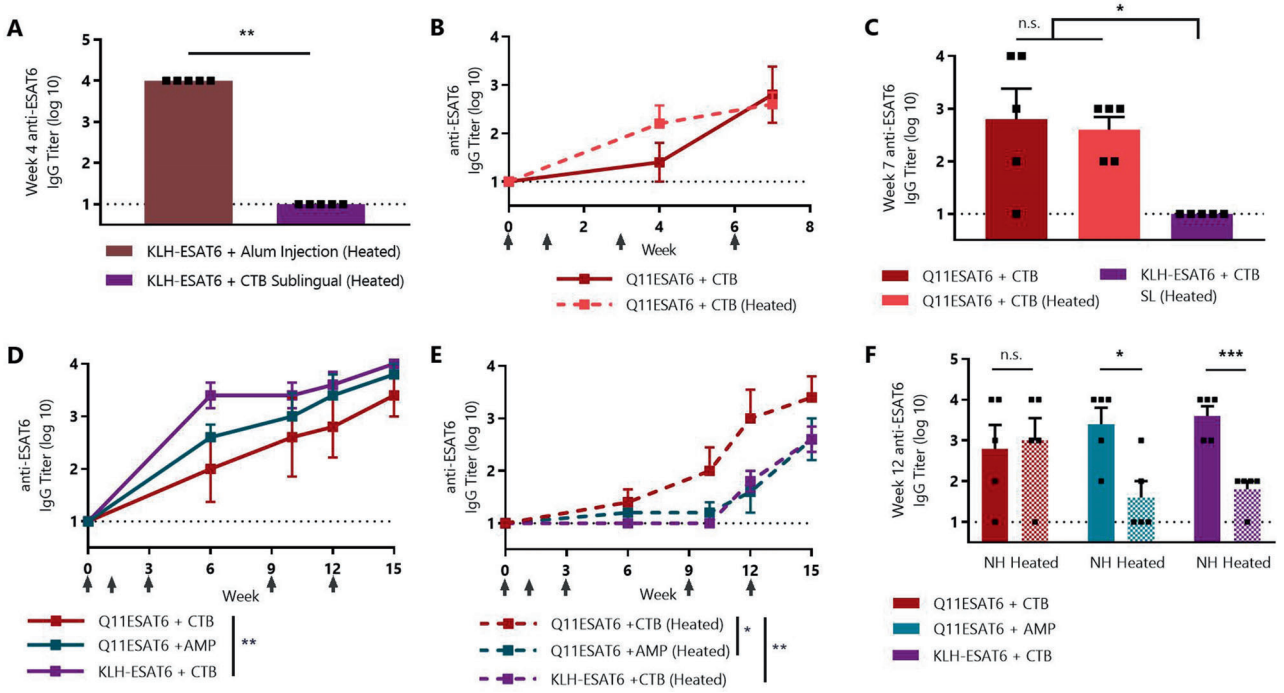

Figure 3. SIMPL tablet vaccine raises antibody responses against *M. tuberculosis* peptide epitope that are not diminished by heating. A) CBA/J mice were immunized subcutaneously with a 1:1 mixture of alum and KLH-ESAT6 or sublingually with KLH-ESAT6 and 10 µg CTB and boosted at week 3. Heated group was heated at 45 °C for 7 days. ** p <0.01 by 1-way ANOVA with Tukey's multiple comparisons test, n = 5/group. B) Mice were immunized with SIMPL tablets containing 20 nmol Q11ESAT6 and 10 µg CTB adjuvant and boosted at weeks 1, 3, and 6. Heated group was heated at 45 °C for 7 days. n = 5/group. C) Comparison of groups from (A) and (B). All groups were boosted at weeks 1, 3, and 6 and week 7 titer is shown. n.s. (not significant) or * p < 0.05 by 1-way ANOVA with Tukey's multiple comparisons test, n = 5/group. D,E) Mice were immunized sublingually with KLH-ESAT6 or Q11ESAT6 and 15 µg CTB or AMP adjuvant and boosted at weeks 1, 3, 9, and 12. Heated groups were heated at 45 °C for 7 days. * p < 0.05, ** p < 0.01 by 2-way ANOVA with Tukey's multiple comparisons test, n = 5/group. F) Serum IgG titers of heated and non-heated (NH) formulations from (D) and (E) were compared. n.s. (not significant), * p < 0.01, *** p < 0.001 by multiple t-tests with Holm-Šidák correction, n=5/group.

difference in response for mice immunized with heated or non-heated Q11ESAT6 + CTB tablets (Figure 3C).

To confirm and extend these findings, we repeated this experiment and tested the use of the nucleotide adjuvant cyclic-di-AMP. We also included a higher dose of adjuvant due to its ability to modulate titers in the tablet immunizations against the pOVA epitope (Figure 2E). Sublingually delivered, non-heated KLH-ESAT6 + CTB raised responses that were the same as tablets adjuvanted with cyclic-di-AMP and slightly higher than tablets adjuvanted with CTB (Figure 3D). The results were dramatically different after heating, however, as CTB-adjuvanted tablets elicited significantly greater antibody levels than the KLH-based vaccine (Figure 3E). We again found that SIMPL tablets containing ESAT6Q11 + CTB were completely unaffected by heating, while KLH + CTB responses were significantly reduced (Figure 3F). Interestingly, tablets containing cyclic-di-AMP adjuvant were not heat-stable, indicating that adjuvant stability is an important consideration even when using a heat-stable vaccine platform. While only serum IgG responses were measured in this study, mucosal IgA responses characteristic of sublingually administered vaccines may also be elicited, though future work is needed to characterize the mucosal responses raised by SIMPL tablets.

In summary, we designed a sublingual tablet vaccine based on self-assembling peptide-polymer nanofibers. These SIMPL tablets represent the first demonstration of a nanomaterial sublingual tablet vaccine to our knowledge. Through addition of sugar excipients and freeze-drying, the tabletization process produced highly porous and easily handleable tablets that raise antibody responses against both the model epitope pOVA and the *M. tuberculosis* epitope ESAT6. The tablets were easily administrable by dissolving under the tongue. In contrast to a conventional KLH-based vaccine, sublingually delivered tablets with CTB adjuvant were heat-stable and showed no loss of immunogenicity after heating at 45 °C for one week. Cyclic-di-AMP adjuvanted tablets did show some loss of potency after heating. Exploring the use of alternate adjuvants or modifications to the tabletization process to preserve the effects of thermally-sensitive adjuvants is an interesting area for future work. For example, we used a relatively low molecular weight of dextran (20 kDa) to promote fast dissolution rates,[25] but higher MW dextran has been shown to promote chemical stability during lyophilization in some cases.[26] Further formulation optimizations may allow for tablets that maximize dissolution rate, tabletability, and immunogenicity. Additionally, focused structural analyses such as circular dichroism or IR spectroscopy could reveal any subtle morphological changes that may occur during tabletization and dissolution. In sum, the thermal stability of SIMPL tablets, combined with their potential for self-administration, shows exciting potential for improving equitable global vaccine distribution.

 © 2021 Wiley-VCH GmbH

Experimental Section

Peptide Synthesis: Peptides were synthesized using Fmoc solid phase synthesis, cleaved with trifluoroacetic acid, and precipitated in diethyl ether prior to purification by RP-HPLC on a C4 column. Conjugation of PEG_{3000} to the C-terminus of OVAQ11 and pOVA and $mPEG_{2000}$ conjugation to the N-terminus of Q11ESAT6 were performed as described.[12] Biotinylation and conjugation of fluorescent TAMRA were performed as described.[27] Peptide identity was confirmed using MALDI mass spectrometry. KLH-ESAT6 conjugates were prepared as described[28] using Cys-ESAT6 peptide and Imject Maleimide Activated mcKLH Kit (Thermo Scientific, cat #77 666).

SIMPL Tabletization Process: Reverse tablet molds were designed in FreeCAD and 3D-printed with a MakerBot Ultimaker 3. PDMS molds were prepared using SYLGARD 184 kits (Sigma, cat #761 028). Peptide solutions were prepared at 2×10^{-3} M in 1X PBS, incubated for 3–4 h at room temperature to fibrillize, and mixed with sugars to a final concentration of 0.67×10^{-3} M peptide and 7.8 wt% each of trehalose (Santa Cruz Biotechnology, cat #394 303), 20 000 Da dextran (Alfa Aesar, cat# J61216), and mannitol (Sigma, cat #M4125). Adjuvanted formulations contained cholera toxin B (List Biological, cat #104) or Vaccigrade cyclic-di-AMP (Invivogen, cat #vac-nacda) at doses indicated in figure captions. Final solutions were pipetted into the PDMS tray (30 µL per tablet), frozen at −80 °C, and lyophilized. Heating was performed by placing individual tablets in microcentrifuge tubes in a heating block set at 45°C. KLH groups were heated as solutions in their final formulation.

MicroCT: Analysis was performed using a Nikon XTH 225 ST instrument, with collection of 2500 projections and an exposure time of 500 ms. Raw data was reconstructed using the Nikon Feldkamp Cone Based CT algorithm and Nikon software. Avizo software was used for 3D reconstructions.

Thioflavin T (ThT) Binding: To measure β-sheet character, 20 µL of 2×10^{-3} M peptide or dissolved tablet solutions were mixed with 180 µL of a 50×10^{-6} M solution of ThT (Alfa Aesar, cat # J61043) in 1X PBS in a black 96-well plate and read using a Molecular Devices Spectramax M2 spectrophotometer (excitation at 440 nm, emission at 488 nm).

Electron Microscopy: Transmission EM was performed as described.[12] For tablet imaging, tablets were dissolved in 1X PBS and samples were immediately prepared to avoid refibrillization.

Micro-Strain Analysis: Tablets were subjected to compressive testing at room temperature using a TA Instruments AIII microstrain-analyzer. The 15 mm size parallel plates corresponding to −81.8 gm ± 1.0 gm force were used. The diameter and height of each tablet was measured, and a compressive force was applied on each tablet for 360 s at an extension rate of −0.003 mm s^{-1}.

In Vitro Uptake Assay: DC2.4 mouse dendritic cells were seeded overnight in a 12 well plate at 1×10^6 cells mL^{-1} (1 mL per well) in complete RPMI media. The next day, 500 µL of media was aspirated and 500 µL of TAMRA-pOVA or media were added to pOVA-treated and untreated wells, respectively. For the tablet group, 500 µL of media was added to each well and the tablets were gently dropped into the wells to dissolve. All groups contained 20 nmol of total peptide per well. After incubation for 2 or 6 h, the cells were prepared for flow cytometry. Cells were treated with Fc blocking antibody (BD Biosciences, cat # 553 141) for 30 min and stained with CD11c:PE-Cy7 (BD Biosciences, cat #561 022) for 30 min. Flow cytometry was performed on a FACS Canto cytometer and data was analyzed using FlowJo software.

In Vitro Activation Assay: DC2.4 cells were seeded overnight in a 48-well plate at 5×10^4 cells per well in complete RPMI media. Cells were treated for 16 h with either 20 nmol of freshly prepared $mPEG_{2000}$–Q11OVA nanofiber solutions or with tablets containing the same quantity of nanofibers. Formulations were unadjuvanted or contained CTB at 50 µg mL^{-1}. Cells were stained with I-A/I-B:FITC (BioLegend, cat #107 606), CD80:PE (BioLegend, cat #104 708), CD86:APC/Cy7 (BioLegend, cat# 105 030), and DAPI. Flow cytometry was performed on a FACS Canto cytometer and data was analyzed using FlowJo software.

Mice and Immunizations: Due to haplotype compatibility, female C57BL/6 mice (Envigo) were used for immunizations against pOVA and female CBA/J mice (Jackson Laboratory) were used for immunizations against ESAT6. Mice were 8–12 weeks at initiation of experiments (age matched within experiments). All animal experiments were performed under Duke University Institutional Care and Use Committee protocol A264-18-11. Sublingual immunizations were performed as previously described;[12] for tablet groups, the tablets were placed under the anesthetized mouse's tongue using silicone-tipped tweezers. Peptide concentration, adjuvant dose, and boosting schedule are described in figure captions. KLH injections were performed as previously described.[28]

Antibody Measurement: Serum ELISAs were performed as previously described.[12] Briefly, plates were coated with streptavidin at 4 °C overnight, followed by incubation with biotin-pOVA or biotin-ESAT6. Plates were blocked, diluted serum was added, and antigen-specific IgG was detected using goat anti-mouse IgG (Jackson Immuno Research, cat #115-035-071).

T-Cell Response Measurement: ELISPOT assays were performed essentially as described.[27] For analysis of lymph node responses, the submandibular and cervical nodes were taken as the draining lymph nodes. Antigen-specific stimulation was performed using the pOVA epitope.

Statistical Analysis: Statistical analysis was performed using the group sizes and statistical tests indicated in the figure legends (1-way or 2-way ANOVA with Tukey's multiple comparison's test; *t*-tests with Holm-Šidák correction), using GraphPad Prism version 7 software. Means ± standard error of the mean (s.e.m.) are presented. Statistically significant differences are indicated in each graph as $*p < 0.05$, $**p < 0.01$, $***p < 0.001$, and $**** p < 0.0001$.

Supporting Information

Supporting Information is available from the Wiley Online Library or from the author.

Acknowledgements

This research was supported by the National Institutes of Health (NIBIB 5R01EB009701; NIAID 5R01AI118182). S.H.K. was supported by the National Science Foundation Graduate Research Fellowship Program under Grant No. DGE-1644868. The MALDI was performed on an instrument supported by North Carolina Biotechnology Center grant 2017-IDG-1018. DC2.4 cells were kindly provided by Dr. Kenneth L. Rock (University of Massachusetts Medical Center, Worcester, MA, USA). 3D-printing resources were provided by the Duke University Innovation Co-Lab.

Conflict of Interest

J.H.C. and S.H.K. are listed as inventors on a patent application associated with the technology described.

Data Availability Statement

The data that support the findings of this study are available from the corresponding author upon reasonable request.

Keywords

biomaterials, self-assembly, sublingual tablets, supramolecular assemblies, vaccine

Received: September 10, 2020
Revised: January 6, 2021
Published online:

 © 2021 Wiley-VCH GmbH

[1] M. Peck, M. Gacic-Dobo, M. S. Diallo, Y. Nedelec, S. S. Sodha, A. S. Wallace, *Morb. Mortal. Wkly. Rep.* **2019**, *68*, 937.
[2] K. De Boeck, C. Decouttere, N. Vandaele, *Omega*, Elsevier, New York **2019**.
[3] A. Ashok, M. Brison, Y. LeTallec, *Vaccine* **2017**, *35*, 2217.
[4] M. M. van den Ent, A. Yameogo, E. Ribaira, C. M. Hanson, R. Ratoto, S. Rasolomanana, C. Foncha, F. Gasse, *Vaccine* **2017**, *35*, 2148.
[5] J. Reina, *Vacunas (English Edition)*, Elsevier, New York **2019**.
[6] H. Kraan, H. Vrieling, C. Czerkinsky, W. Jiskoot, G. Kersten, J.-P. Amorij, *J. Controlled Release* **2014**, *190*, 580.
[7] L. Yenkoidiok-Douti, C. M. Jewell, *ACS Biomater. Sci. Eng.* **2020**, *6*, 759.
[8] C. N. Fries, E. J. Curvino, J.-L. Chen, S. R. Permar, G. G. Fouda, J. H. Collier, *Nat. Nanotechnol.* **2020**, https://doi.org/10.1038/s41565-020-0739-9.
[9] B. Cossette, S. H. Kelly, J. H. Collier, *ACS Biomater. Sci. Eng.* **2020**, https://doi.org/10.1021/acsbiomaterials.0c01291.
[10] M.-N. Kweon, in *Mucosal Vaccines*, 2nd ed. (Eds: H. Kiyono, D. W. Pascual), Academic Press, San Diego, CA **2020**, pp. 477–486.
[11] S. K. Lai, Y.-Y. Wang, J. Hanes, *Adv. Drug Delivery Rev.* **2009**, *61*, 158.
[12] S. H. Kelly, Y. Wu, A. K. Varadhan, E. J. Curvino, A. S. Chong, J. H. Collier, *Biomaterials* **2020**, *241*, 119903.
[13] J. S. Wilkhu, S. E. McNeil, D. E. Anderson, M. Kirchmeier, Y. Perrie, *Eur. J. Pharm. Sci.* **2017**, *108*, 71.
[14] R. Chandrasekhar, Z. Hassan, F. AlHusban, A. M. Smith, A. R. Mohammed, *Eur. J. Pharm. Biopharm.* **2009**, *72*, 119.
[15] S. V. Sastry, J. R. Nyshadham, J. A. Fix, *Pharm. Sci. Technol. Today* **2000**, *3*, 138.
[16] S. Ohtake, Y. J. Wang, *J. Pharm. Sci.* **2011**, *100*, 2020.
[17] J. S. Rudra, T. Sun, K. C. Bird, M. D. Daniels, J. Z. Gasiorowski, A. S. Chong, J. H. Collier, *ACS Nano* **2012**, *6*, 1557.
[18] Y. Wen, J. H. Collier, *Curr. Opin. Immunol.* **2015**, *35*, 73.
[19] H.-J. Cho, J.-Y. Kim, Y. Lee, J. M. Kim, Y. B. Kim, T. Chun, Y.-K. Oh, *Vaccine* **2010**, *28*, 2598.
[20] C. Mora-Solano, Y. Wen, H. Han, J. Chen, A. S. Chong, M. L. Miller, R. R. Pompano, J. H. Collier, *Biomaterials* **2017**, *149*, 1.
[21] W. H. Organization, *Global Tuberculosis Report*, World Health Organization, Geneva **2017**. Contract No.: WHO/HTM/TB 2017.
[22] A. Weinreich Olsen, P. R. Hansen, A. Holm, P. Andersen, *Eur. J. Immunol.* **2000**, *30*, 1724.
[23] W. H. Organization, *Temperature Sensitivity of Vaccines*, World Health Organization, **2006**.
[24] P. Van Damme, M. Cramm, A. Safary, P. Vandepapeliere, A. Meheus, *Vaccine* **1992**, *10*, 366.
[25] L. Casettari, G. Bonacucina, G. A. Morris, D. R. Perinelli, P. Lucaioli, M. Cespi, G. F. Palmieri, *Powder Technol.* **2015**, *273*, 125.
[26] S. Yoshioka, Y. Aso, S. Kojima, *Pharm. Res.* **1997**, *14*, 736.
[27] Y. Wu, P. K. Norberg, E. A. Reap, K. L. Congdon, C. N. Fries, S. H. Kelly, J. H. Sampson, V. P. Conticello, J. H. Collier, *ACS Biomater. Sci. Eng.* **2017**, *3*, 3128.
[28] T. Sun, H. Han, G. A. Hudalla, Y. Wen, R. R. Pompano, J. H. Collier, *Acta Biomater.* **2016**, *30*, 62.

© 2021 Wiley-VCH GmbH

Supplementary Tables

Supplementary Table.1 Summary of *Cordata(Willd.) R.* Br. Leaf cDNA library sequencing results

Result Name	Number	Length (bp)
Sequenced ESTs	883	/
High quality ESTs	511	/
Non-redundant sequences (singltons+clusters)	364	/
Number of clusters	78	/
Number of ESTs in clusters	223	/
Number of singltons	286	/
Average sequences/clusters	3.62	/
Average non-redundant sequence size	/	513
Shortest non-redundant sequence size	/	105
Longest non-redundant sequence size	/	1013

Supplementary Table.2 The KEGG profiles of transcripts from *Macleaya cordata*

Pathway	Enzyme	Enzyme ID	Seqs
Glycolysis / Gluconeogenesis	alcohol dehydrogenase	ec:1.1.1.1	1
Fatty acid degradation	alcohol dehydrogenase	ec:1.1.1.1	1
Glycine, serine and threonine metabolism	alcohol dehydrogenase	ec:1.1.1.1	1
Tyrosine metabolism	alcohol dehydrogenase	ec:1.1.1.1	1
Retinol metabolism	alcohol dehydrogenase	ec:1.1.1.1	1
Chloroalkane and chloroalkene degradation	alcohol dehydrogenase	ec:1.1.1.1	1
Drug metabolism - cytochrome P450	alcohol dehydrogenase	ec:1.1.1.1	1
Metabolism of xenobiotics by cytochrome P450	alcohol dehydrogenase	ec:1.1.1.1	1
Naphthalene degradation	alcohol dehydrogenase	ec:1.1.1.1	1
Butanoate metabolism	hydroxybutyrate dehydrogenase	ec:1.1.1.30	1
Synthesis and degradation of ketone bodies	hydroxybutyrate dehydrogenase	ec:1.1.1.30	1
Valine, leucine and isoleucine degradation	3-hydroxyisobutyrate dehydrogenase	ec:1.1.1.31	1

Pentose phosphate pathway	phosphogluconate dehydrogenase (NADP+-dependent, decarboxylating)	ec:1.1.1.44	2
Glutathione metabolism	phosphogluconate dehydrogenase (NADP+-dependent, decarboxylating)	ec:1.1.1.44	2
Glyoxylate and dicarboxylate metabolism	2-hydroxy-3-oxopropionate reductase	ec:1.1.1.60	1
Oxidative phosphorylation	ubiquinol---cytochrome-c reductase	ec:1.10.2.2	2
Arachidonic acid metabolism	monooxygenase	ec:1.14.14.1	1
Fatty acid degradation	monooxygenase	ec:1.14.14.1	1
Linoleic acid metabolism	monooxygenase	ec:1.14.14.1	1
Steroid hormone biosynthesis	monooxygenase	ec:1.14.14.1	1
Tryptophan metabolism	monooxygenase	ec:1.14.14.1	1
Retinol metabolism	monooxygenase	ec:1.14.14.1	1
Caffeine metabolism	monooxygenase	ec:1.14.14.1	1
Aminobenzoate degradation	monooxygenase	ec:1.14.14.1	1
Drug metabolism - cytochrome P450	monooxygenase	ec:1.14.14.1	1
Metabolism of xenobiotics by cytochrome P450	monooxygenase	ec:1.14.14.1	1
Steroid biosynthesis	7-dehydrocholesterol reductase	ec:1.3.1.21	2
Vitamin B6 metabolism	pyridoxal 5'-phosphate synthase	ec:1.4.3.5	1
Oxidative phosphorylation	NADH:ubiquinone reductase (H^+-translocating)	ec:1.6.5.3	2
Oxidative phosphorylation	NADH dehydrogenase	ec:1.6.99.3	1
Sulfur metabolism	phosphoadenylyl-sulfate reductase (thioredoxin)	ec:1.8.4.8	1
Sulfur metabolism	adenylyl-sulfate reductase (glutathione)	ec:1.8.4.9	1
Sulfur metabolism	adenosine 5'-phosphosulfate	ec:1.8.99.2	1

	reductase		
Oxidative phosphorylation	cytochrome-c oxidase	ec:1.9.3.1	1
Glycerophospholipid metabolism	phosphoethanolamine N-methyltransferase	ec:2.1.1.103	1
Lysine degradation	histone-lysine N-methyltransferase	ec:2.1.1.43	1
Pentose phosphate pathway	transketolase	ec:2.2.1.1	1
Carbon fixation in photosynthetic organisms	transketolase	ec:2.2.1.1	1
Biosynthesis of ansamycins	transketolase	ec:2.2.1.1	1
Sulfur metabolism	serine O-acetyltransferase	ec:2.3.1.30	1
Cysteine and methionine metabolism	serine O-acetyltransferase	ec:2.3.1.30	1
Galactose metabolism	galactinol synthase	ec:2.4.1.123	1
Purine metabolism	adenine phosphoribosyltransferase	ec:2.4.2.7	1
N-Glycan biosynthesis	dolichyl-diphosphooligosaccharide---protein glycotransferase	ec:2.4.99.18	1
Glutathione metabolism	glutathione transferase	ec:2.5.1.18	2
Drug metabolism - cytochrome P450	glutathione transferase	ec:2.5.1.18	2
Metabolism of xenobiotics by cytochrome P450	glutathione transferase	ec:2.5.1.18	2
Cysteine and methionine metabolism	S-adenosylmethionine synthetase	ec:2.5.1.6	2
Plant-pathogen interaction	LRR receptor-like serine/threonine-protein kinase FLS2	ec:2.7.11.1	2
MAPK signaling pathway	mitogen-activated protein kinase	ec:2.7.11.24	2
Purine metabolism	nucleoside-diphosphate kinase	ec:2.7.4.6	1
Pyrimidine metabolism	nucleoside-diphosphate kinase	ec:2.7.4.6	1
Sulfur metabolism	adenylyltransferase	ec:2.7.7.4	1

Purine metabolism	adenylyltransferase	ec:2.7.7.4	1
Selenocompound metabolism	adenylyltransferase	ec:2.7.7.4	1
Methane metabolism	phosphoserine phosphatase	ec:3.1.3.3	1
Glycine, serine and threonine metabolism	phosphoserine phosphatase	ec:3.1.3.3	1
Amino sugar and nucleotide sugar metabolism	chitinase	ec:3.2.1.14	1
Arginine and proline metabolism	N-carbamoylputrescine amidase	ec:3.5.1.53	1
Purine metabolism	microtubule-severing ATPase	ec:3.6.4.3	1
Glyoxylate and dicarboxylate metabolism	ribulose 1,5-bisphosphate carboxylase/oxygenase	ec:4.1.1.39	2
Carbon fixation in photosynthetic organisms	ribulose 1,5-bisphosphate carboxylase/oxygenase	ec:4.1.1.39	2
Cysteine and methionine metabolism	S-adenosylmethionine decarboxylase	ec:4.1.1.50	1
Propanoate metabolism	malonyl-CoA decarboxylase	ec:4.1.1.9	1
beta-Alanine metabolism	malonyl-CoA decarboxylase	ec:4.1.1.9	1
Nitrogen metabolism	carbonic anhydrase	ec:4.2.1.1	1
Isoquinoline alkaloid biosynthesis	(S)-norcoclaurine synthase	ec:4.2.1.78	1
Ubiquitin mediated proteolysis	peptidyl-prolyl cis-trans isomerase	ec:5.2.1.8	1
Aminoacyl-tRNA biosynthesis	glycyl-tRNA synthetase / glycine--tRNA ligase	ec:6.1.1.14	1
Glyoxylate and dicarboxylate metabolism	glutamine synthetase	ec:6.3.1.2	1
Nitrogen metabolism	glutamine synthetase	ec:6.3.1.2	1
Alanine, aspartate and glutamate metabolism	glutamine synthetase	ec:6.3.1.2	1
Arginine and proline metabolism	glutamine synthetase	ec:6.3.1.2	1
Circadian rhythm – plant	ubiquitin---protein ligase	ec:6.3.2.19	2

Alanine, aspartate and glutamate metabolism	argininosuccinate synthase	ec:6.3.4.5	1
Arginine and proline metabolism	argininosuccinate synthase	ec:6.3.4.5	1

Supplementary Table 3 Theoretical pI/Mw of McDef1-5

Protein	**MASS(Da)**			**pI**		
	precursor	signal	mature	precursor	signal	mature
McDef1	9645.31	2596.18	7067.15	8.73	9.35	8.52
McDef2	10286.92	3404.16	6900.78	8.15	10	7.05
McDef3	10276.88	3394.12	6900.78	8.15	10	7.05
McDef4	10303.91	3408.15	6913.77	6.86	10	6.02
McDef5	10302.97	3408.15	6912.83	8.15	10	7.05

Supplementary Figure legends

Supplementary Figure 1 The length distribution of ESTs.

Supplementary Figure 2 The results of analysis of the Gene Ontology (GO)

Supplementary Figure 3 Analysis of the Cluster of Orthologous Groups (A: RNA processing and modification B: Chromatin Structure and dynamics C: Energy production and conversion D: Cell cycle control and mitosis E Amino Acid metabolism and transport F Nucleotide metabolism and transport G: Carbohydrate metabolism and transport H: Coenzyme metabolism I: Lipid metabolism J: Translation K: Transcription L: Replication and repair M: Cell wall/membrane/envelop biogenesis N: Cell motility O: Post-translational modification, protein turnover, chaperone functions P: Inorganic ion transport and metabolism Q: Secondary Structure T: Signal Transduction U: Intracellular trafficking and secretion Y: Nuclear structure Z: Cytoskeleton R General Functional Prediction only S: Function Unknown).

Supplementary Figure 4. Sequence alignment of McNCS 1

Supplementary Figure 5. Sequence alignment of Mac-co 1

Supplementary Figure 6. The phylogenetic tree of (S)-norcoclaurine synthase and major allergen protein

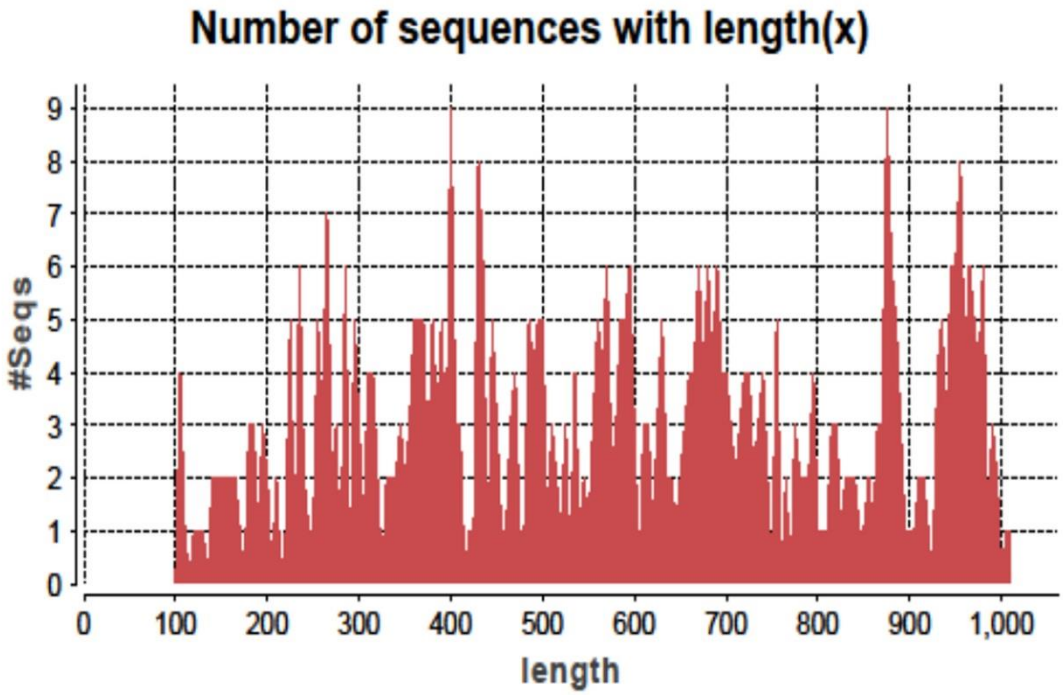

Supplementary Figure 1

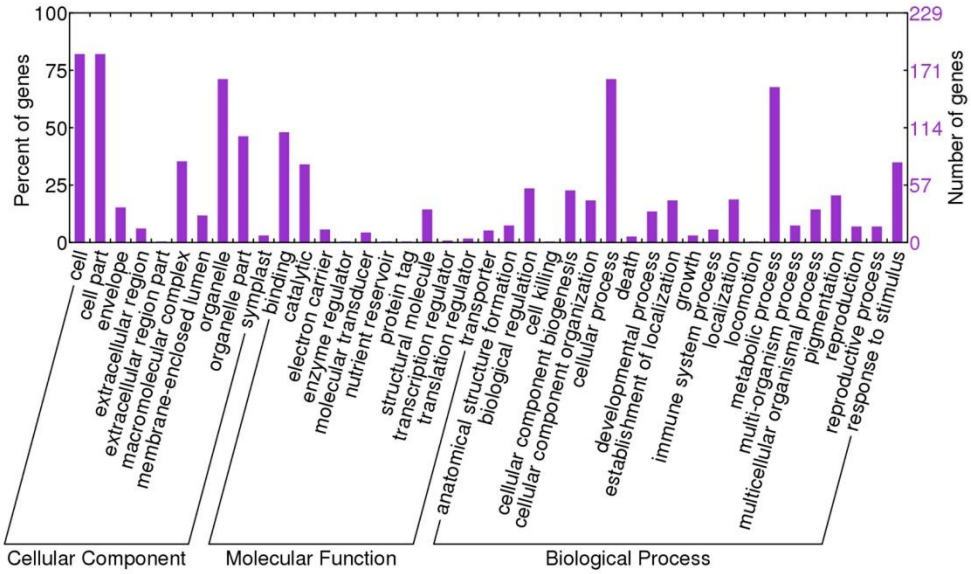

Supplementary Figure 2

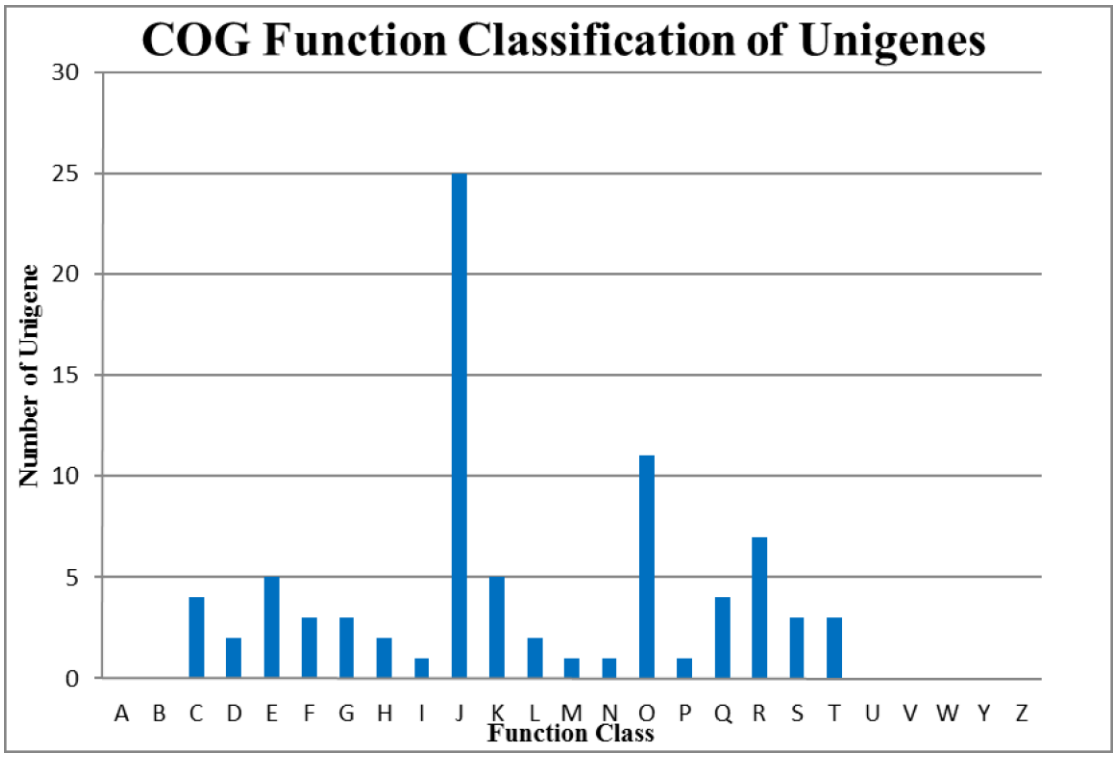

Supplementary Figure 3

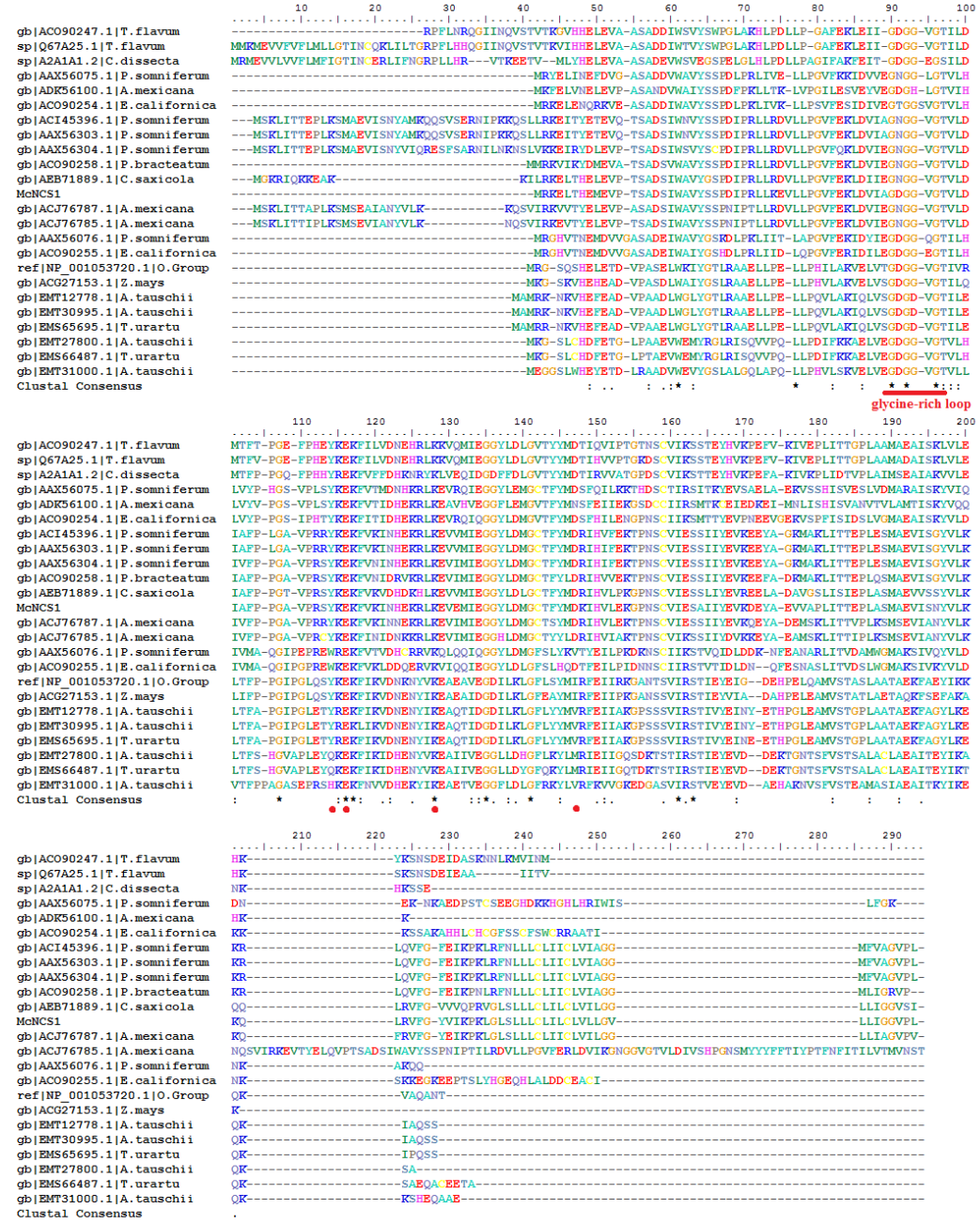

Supplementary Figure 4

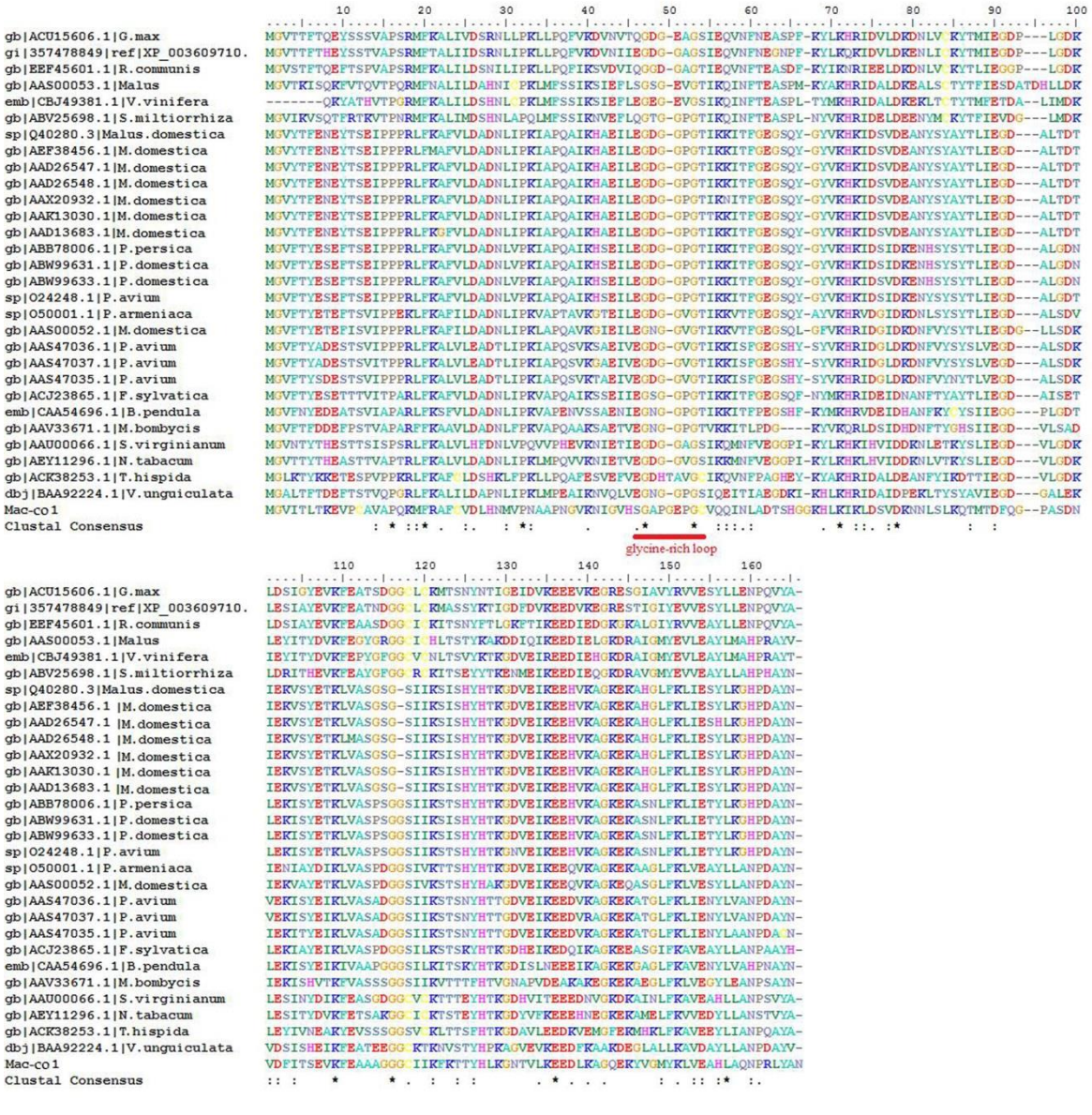

Supplementary Figure 5

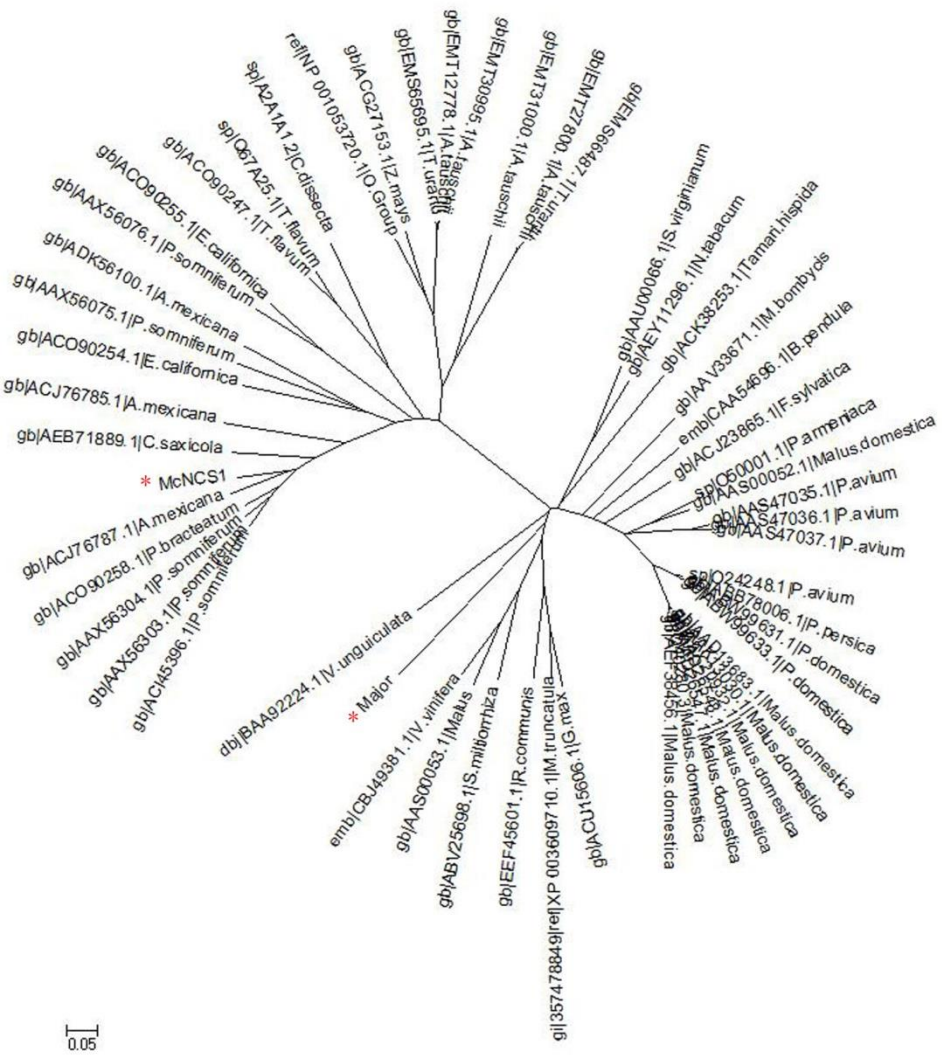

Supplementary Figure 6 The phylogenetic relationship of (S)-norcoclaurine synthase and major allergen protein.